


Electrical parameter estimation of the soil using GPR and full waveform inversion: a case study in Colombia

Jheyston Serrano-Luna^{1*}; Ana Ramírez-Silva¹; Sergio Abreo-Carrillo¹

¹Grupo de Investigación en Conectividad y Procesamiento de Señales - CPS, Escuela de Ingeniería Eléctrica, Electrónica y de Telecomunicaciones (E3T), Universidad Industrial de Santander, Bucaramanga, Colombia. (*) jheyston.serrano@e3t.uis.edu.co; anaberam@uis.edu.co; abreosergio@gmail.com

Abstract

A method of Full Waveform Inversion on GPR data for the estimation of subsurface electrical properties such as relative permittivity and conductivity is proposed in this paper. The GPR radar antenna used for subsurface data acquisition is a B-scan acquisition and it operates at a center frequency of 400 MHz. B-scan acquisitions are a challenge in the subsurface parameter estimation process due to lack of illumination. In addition, B-scan acquisitions are more sensitive to the starting point in estimating subsurface parameters in comparison to multiple offset acquisitions. However, despite the challenges, this type of acquisition is used because it allows portability in areas of difficult access and quick data collection, reducing processing times and costs. In this work, Full Waveform Inversion with cost function constraints was evaluated to estimate subsurface relative permittivity and conductivity using B-scan acquisitions. The proposed methods were evaluated using data collected in a study area located in Mogotes, Santander, Colombia. From the results obtained, it can be concluded that the use of regularization in the inversion process gives smoother subsurface models, also preserving discontinuities. In addition, the incoherent noise in the data is reduced by Gaussian regularization, allowing a better interpretation of the study area.

Keywords: Relative permittivity; Conductivity; Regularizations; FWI; B-scan.

Estimación de propiedades eléctricas del subsuelo usando GPR e inversión de onda completa: un caso de estudio en Colombia

Resumen

En este artículo se propone un método para la estimación de las propiedades eléctricas del subsuelo, tales como permitividad relativa y conductividad, usando inversión de onda completa sobre datos de GPR. La antena de radar GPR que se usó para la adquisición de los datos del subsuelo es de un solo canal y opera a una frecuencia central de 400 MHz. El uso de este tipo de antena implica diferentes desafíos en el proceso de estimación de parámetros del subsuelo debido a la insuficiente iluminación. Además, las adquisiciones con antenas de un solo canal y de compensación corta, son más sensibles al punto de partida en la estimación de parámetros del subsuelo, en comparación con las adquisiciones de compensación múltiple. Sin embargo, a pesar de los desafíos, se utiliza este tipo de adquisición, ya que permite la portabilidad en áreas de difícil acceso, además de una rápida toma de datos, lo cual reduce tiempos y costos de procesamiento. En este trabajo se evaluó la inversión de forma de onda completa, con restricciones en la función de costo para estimar la permitividad relativa y la conductividad del subsuelo usando adquisiciones de un solo canal. Los métodos propuestos se evaluaron usando datos recolectados en una zona de estudio ubicada en Mogotes, Santander, en

How to cite: Serrano-Luna, J.; Ramírez-Silva, A.; Abreo-Carrillo, S. (2023). Electrical parameter estimation of the soil using GPR and full waveform inversion: a case study in Colombia. *Boletín de Geología*, 45(2), 131-144. <https://doi.org/10.18273/revbol.v45n2-2023008>

Colombia. A partir de los resultados obtenidos, se puede concluir que el uso de la regularización en el proceso inverso contribuye a que la solución sean modelos del subsuelo más suaves, que preservan también las discontinuidades. Además, el ruido incoherente en las imágenes del subsuelo se reduce mediante la regularización gaussiana, lo cual permite una mejor interpretación del área de estudio.

Palabras clave: Permittividad relativa; Conductividad; Regularizaciones; FWI; B-scan.

Introduction

Ground Penetrating Radar (GPR) is a standard geophysical method used to identify shallow materials of the subsurface (<100 m). The GPR method is based on electromagnetic waves that are used to determine the properties of the soil, such as relative permittivity and conductivity. In general, the soil can be well characterized through relative permittivity and conductivity since they are indicators of the nature of the soil, moisture content, temperature, and the general geological structure. Those measures are also used to determine the texture of a surface layer because small particles of clay material increase the conductivity of the layer. Such characterization has relevance in applications such as ice analysis, mines and tunnels detection, pavement condition assessment and soil analysis for agriculture and, oil and gas exploration (Daniels, 2004).

In this case, the inverse problem consists of the determination or estimation of the profiles of relative permittivity and conductivity of the soil from data acquired at the surface. Recently, Full Waveform Inversion (FWI), has been used as a local optimization technique that allows estimating physical subsurface parameters from a set of observations at the surface. FWI has been applied in different contexts like seismic (Bunks *et al.*, 1995), seismology (Blom *et al.*, 2020), medical imaging (Guasch *et al.*, 2020; Lucka *et al.*, 2021), and electromagnetics (Lambot *et al.*, 2004; Klotzsche *et al.*, 2010; Mozaffari *et al.*, 2020; Serrano *et al.*, 2020).

The use of FWI with GPR data has many challenges, such as the initial model, the lack of sufficient illumination in the acquisition that produces high wavenumbers in the estimation of the parameters, the crosstalk between parameters, the high computational cost, and finally, the inverse problem is ill-conditioned and ill-posed. In this work, we propose a FWI method with two different regularizations that reduce the incoherent noise present in the data and produce a more stable solution. The proposed methods is tested in real

GPR data collected in the municipality of Mogotes, Santander, in Colombia.

Theoretical framework

The Ground Penetrating Radar (GPR) is an electromagnetic method with applications in geophysics, civil engineering, and archeology (Daniels, 2004; Linde *et al.*, 2010). The transmitter antenna emits an electromagnetic pulse into the soil, where the changes in the subsurface's magnetic and electrical properties generate reflected, refracted, and transmitted energy. In a B-Scan acquisition, a set of consecutive radar waveform record along a particular direction, the energy is measured by one receiver antenna at some distance from the transmitter antenna. Figure 1A shows the principle of operation of a GPR system. Figure 1B shows the trajectories between the transmitter and receiver antennas using ray theory. The trajectories are air wave (AW); ground wave (GW); reflected wave (RW), and critically refracted wave (CRW). The AW trajectory is a direct wave, and its velocity is the speed of light in the air. The GW propagates slower than the AW, and it is a surface wave. The RW is generated by the changes in the electromagnetic parameters of the subsurface (relative permittivity, relative permeability, or conductivity). According to Snell's law, the CRW is generated at the critical angle.

Full waveform inversion

Full waveform inversion (FWI) is an iterative method that is being largely used to determine high-resolution models of the Earth's subsurface from data acquired at the surface. The models of the soil are estimated by minimizing the difference between the recorded and modeled data. For the electromagnetic case, the relative permittivity $\epsilon_r(r)$, and conductivity models $\sigma_r(r)$ can be estimated from the electromagnetic scan measured at the receiving antenna. The method starts at iteration $k=0$, with an initial model m^0 for both parameters, and it is then updated iteratively by the method of Goldstein (1965).

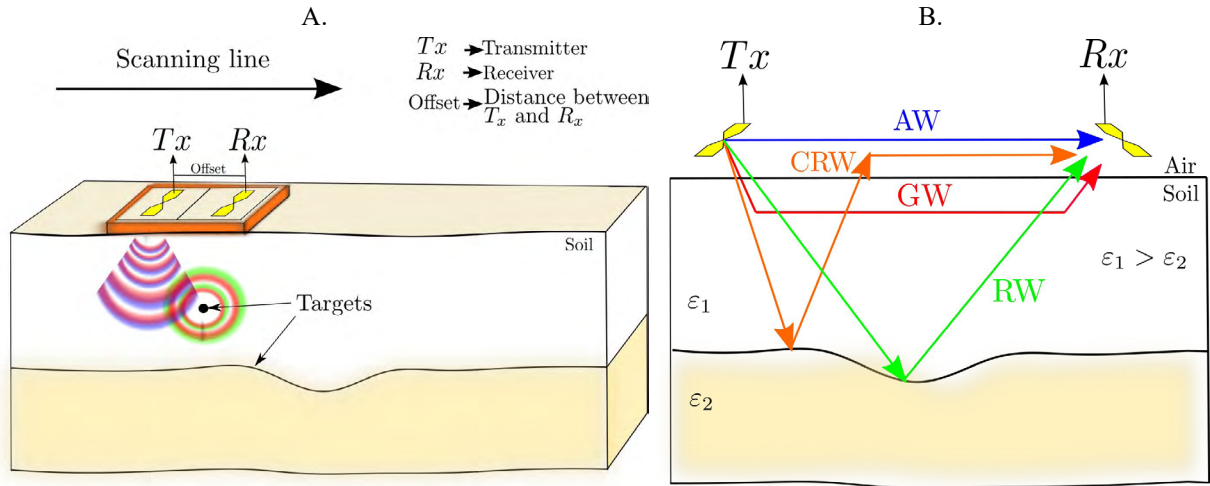


Figure 1. A. The principle of operation of a GPR system with two layers of contrasting permittivity (ϵ_1 and ϵ_2), modified from Persico (2014). B. Signal trajectories: air wave (AW), ground wave (GW), reflected wave (RW) and critical refracted wave (CRW); modified from Jol (2008).

$$m^{k+1} = m^k + \alpha_k \Delta m^k, \quad (1)$$

where α_k is the step size and $\Delta m^k = -g(m^k)$ is the gradient evaluated at m^k . Each parameter is updated using the gradient function as follows

$$g(\epsilon_r(r)) = \int_0^T \epsilon_0 \lambda_{E_y}(r, t) \frac{\partial E_y(r, t)}{\partial t} dt, \quad (2)$$

$$g(\sigma_r(r)) = \int_0^T \sigma_0 \lambda_{E_y}(r, t) E_y(r, t) dt, \quad (3)$$

where $E_y(r, t)$ is the electric field in the y -direction (V/m), ϵ_0 is the permittivity in the vacuum and σ_0 is a regularization value. Also, in Equations 2 and 3, $\lambda_{E_y}(r, t)$ is an adjoint field that simulates electromagnetic wave propagation but in reverse time. T is the final time of electromagnetic wave propagation.

$$\Phi_{GS2}(s, m, \varrho) = \frac{1}{2} \left\| v(\varrho, scans) * \left(\frac{d_{mod}(s, t) \|d_{obs}(t)\|_2}{\|d_{mod}(s, t)\|_2} - d_{obs}(t) \right) \right\|_2^2, \quad (4)$$

where $v(\varrho, scans)$ is a Gaussian function with standard deviation ϱ . The Gaussian function $v(\varrho, scans)$ is convolved with the difference between the modeled and observed data. The Gaussian function is defined as

$$v(\varrho, t) = \frac{1}{\sqrt{2\pi}\varrho} e^{-\frac{(t - Taux)^2}{2\varrho^2}}, \quad (5)$$

Methodology

FWI with Gaussian function

The estimation of the electromagnetic soil parameters is proposed, in this work, via three different alternative cost functions for FWI. The first alternative cost function uses a Gaussian window. According to Xue *et al.* (2016), a smoothing parameter in the cost function allows for improving its convexity. FWI is a local optimization technique where the convexity of the cost function is desirable to avoid being trapped in local minima. The method proposed by Xue *et al.* (2016) uses a small number of misfit functions with smoothing kernels of decreasing strengths; during the FWI process, this allows the estimation of high-quality models with starting points that do not have enough low-frequency information. We have adapted the cost function to include the Gaussian function in the scan-directions, which is given by

where $T_{aux} = \frac{T - dt}{2}$, t is the time vector, and T is the width of the Gaussian function. If the parameter ϱ^2 is large, the cost function is not multimodal, which allows ignoring high-frequency information of the data. On the contrary, if the parameter ϱ^2 is small, the cost function is multimodal, and the noise in the data together with an initial model without sufficient low-frequency information produces a noisy solution. The

Gaussian function helps converge to a solution of low wavenumbers that depend on the width of the window and the parameter ϱ .

FWI with Total Variation (TV) regularization

The second alternative for the cost function for FWI is the regularization of total variation (TV), used to

$$\Phi_{TV}(s, m) = \frac{1}{2} \left\| \frac{d_{mod}(s) \| d_{obs} \|_2}{\| d_{mod}(s) \|_2} - d_{obs} \right\|_2^2 + \lambda_{TV} \sum_j^{Nx} \sum_i^{Nz} \left(\sqrt{(D_x^{m_{i,j}})^2 + (D_z^{m_{i,j}})^2 + \alpha_{TV}^2} \right), \quad (6)$$

where $D_x^{m_{i,j}} = m_{i+1,j} - m_{i,j}$, $D_z^{m_{i,j}} = m_{i,j+1} - m_{i,j}$ and α_{TV} is a small constant to avoid the numerical division by zero in the gradient.

FWI with Modified Total Variation (MTV) regularization

The modified total variation (MTV) is proposed by Lin and Huang (2014) as an alternative regularization

$$\min_{\mathbf{m}, \mathbf{u}} \Phi_d(s, \mathbf{m}, \mathbf{u}) = \frac{1}{2} \left\| \frac{\mathbf{d}_{mod}(s) \| \mathbf{d}_{obs} \|_2}{\| \mathbf{d}_{mod}(s) \|_2} - \mathbf{d}_{obs} \right\|_2^2 + \lambda_{MTV|1} \| \mathbf{m} - \mathbf{u} \|_2^2 + \lambda_{MTV|2} \| \mathbf{u} \|_{TV}; \quad (7)$$

with

$$\lambda_{MTV|1} = \gamma_{MTV} \frac{\| g(\mathbf{m}^k) \|_2}{\| \mathbf{m}^k - \mathbf{u}^{k-1} \|_2}, \lambda_{MTV|2} = \frac{\max(|\mathbf{m}^k - \mathbf{u}^{k-1}|)}{k}, \quad (8)$$

where γ_{MTV} can take values from 0.05 to 0.5 and k can take values from 0 to 200 according to Gao and Huang (2019). A large value of γ_{MTV} does not generate changes in the estimated parameters. On the other hand, a small value of the γ_{MTV} regularization results in the traditional FWI solution. Small values of k result in the traditional FWI solution, whereas a very high value for k results in a very smooth solution.

Experimental Results

Description of the experiment

The proposed methods are evaluated in the estimation of the electromagnetic soil parameters of a small area, located in Mogotes, a local municipality in the department of Santander, Colombia. The raw GPR data is acquired using a shielded antenna with a central frequency of 400 MHz. The acquisition line is shown

reduce the noise contamination of the data (Rudin *et al.*, 1992; Rodríguez, 2013). TV regularization seeks to obtain a smooth estimate while preserving the main structures. The cost function for FWI using TV regularization is given by Anagaw and Sacchi (2012).

method. The MTV regularization is a more stable version of TV since it does not depend on the α_{TV}^2 value included to avoid divisions by zero in the gradients. The MTV method is selected in B-scan acquisition as the first step to obtaining low wavenumbers in the image, which is difficult to obtain due to the lack of illumination during the acquisition. The MTV method is dictated by solving the following cost function

in Figure 2A; it was selected near the Mogoticos river, where a visible outcrop is accessible. In the outcrop, two continuous geological layers of different rock materials are visible (Figure 2B). The acquisition includes 213 scans spaced 0.1 m. The total propagation time of the scan is 99.99 ns with 512 samples, and a time step of 0.195 ns. The acquisition line has a total length of 21.3 m.

Initial permittivity and conductivity

The first step to estimate the soil parameters is to determine an initial guess for the type of rock materials. For the area under study, only permittivity and conductivity were considered, and permeability is not taken into account. Picking the first wave arrival in the raw data is performed to find three significant reflectors, as shown in Figure 3. Then, the relative permittivity and conductivity values are selected

taking into account the typical values of the subsurface materials and a visual inspection: in layer-A, the relative permittivity is 4, and conductivity is 1 mS/m, the material is considered a dry clayey soil. In layer-B, the relative permittivity is selected as dry-sand with

a value equal to 6 and the conductivity is 1 mS/m; finally, the layer-C is chosen to be wet clay, and the relative permittivity value is 12 with conductivity of 4 mS/m.

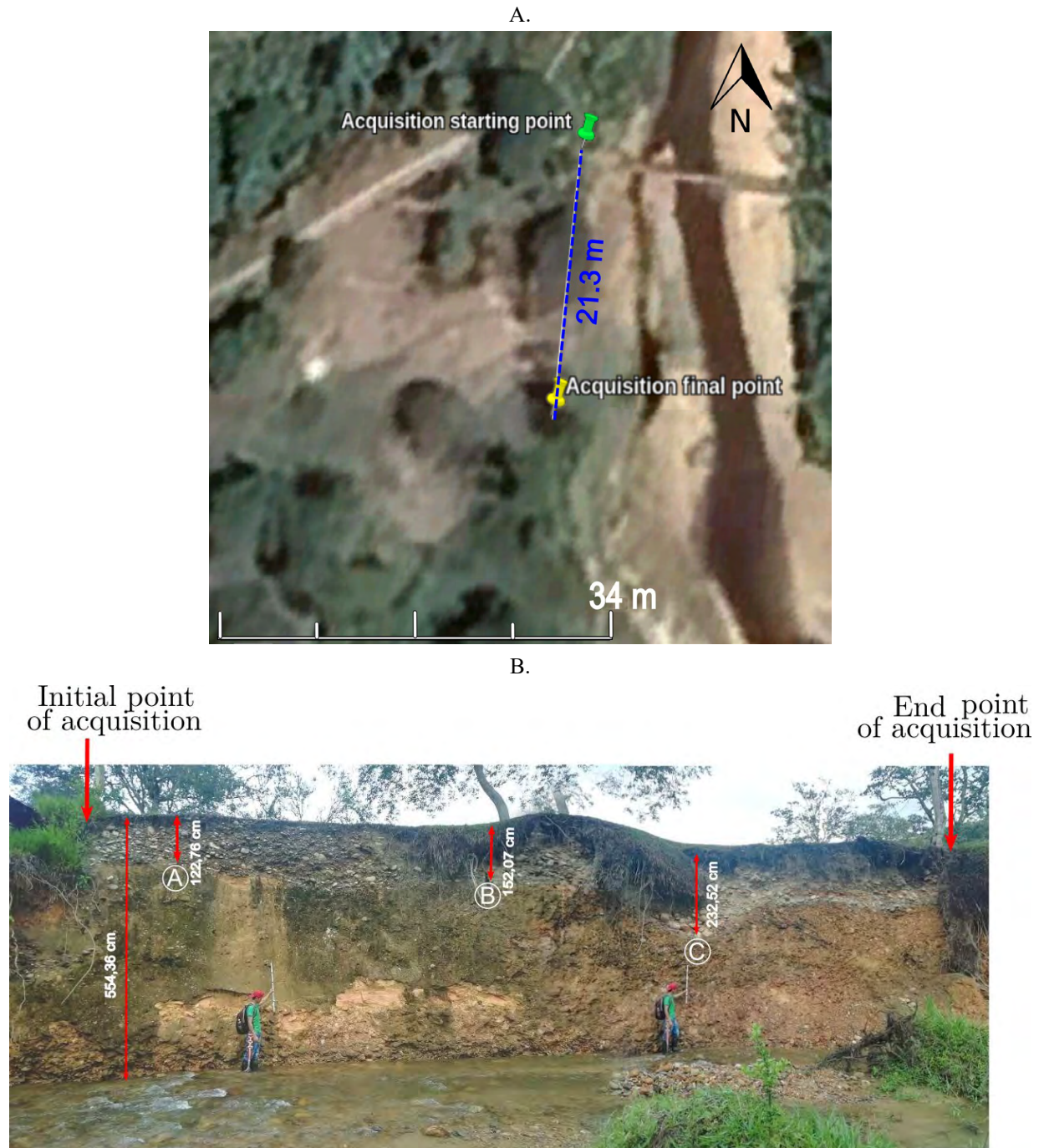


Figure 2. A. Acquisition line. B. Outcrop in the acquisition zone with three layers based on visual inspection: dry clay, dry sand, and wet clay soil, from top to bottom.

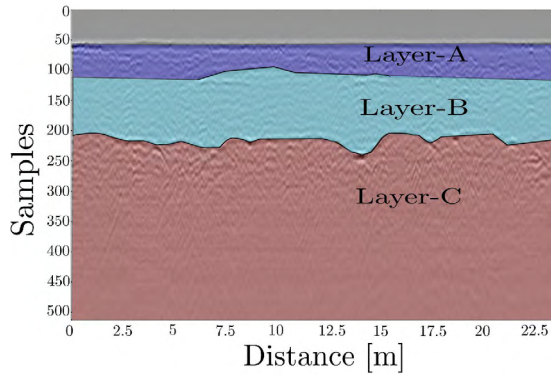


Figure 3. Raw GPR data interpretation with three continuous layers based on main reflectors: dry clay (layer-A), dry sand (layer-B) and wet clay (layer-C) soil.

The depth of each layer is obtained with the picking time and the relative permittivity of each layer. The first depth layer is computed using Equation 9 and the depths of the second and third layers are computed using Equation 10.

$$D_l = \frac{c(t_l - t_{air})}{2\sqrt{\epsilon_{r,l}(\mathbf{r})}}, \quad (9)$$

$$D_l = D_{l-1} + \frac{c(t_l - t_{l-1})}{2\sqrt{\epsilon_{r,l}(\mathbf{r})}} \quad (10)$$

In Equations 9 and 10, l is the layer index, t_l is the picking of the first wave arrival of the signal with higher amplitude, t_{air} is the time for the air wave (approx. 0.9375 ns), c is the velocity of electromagnetic waves in the vacuum, which is 3×10^8 m/s, and $\epsilon_{r,l}$ is the relative permittivity in layer l .

Figures 4A and 4C illustrate the permittivity and conductivity models for the layers. The spatial step of the images displayed in Figure 4 is 0.025 m in x- and z-directions. Figures 4B and 4D show the permittivity and conductivity models smoothed by a blurring filter of size 5×5 .

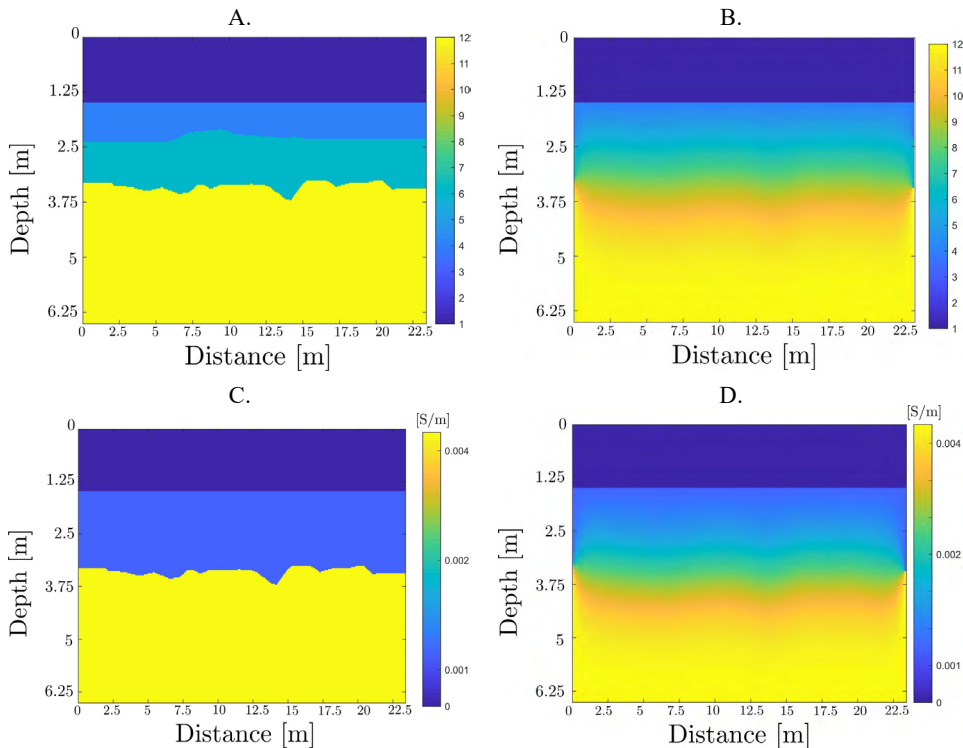


Figure 4. Initial guess for the electromagnetic parameters. **A.** Relative permittivity. **B.** Initial relative permittivity obtained after applying a smoothing filter on the model illustrated in Figure 4A. **C.** Conductivity. **D.** Initial conductivity obtained after applying a smoothing filter on the model illustrated in Figure 4C.

Source wavelet estimation using the impulse response

In the GPR scenario of a B-scan acquisition, the antenna is located in the air, and the sign source can be estimated from the air-wave. The relationship of the source with the data in the air wave is linear; therefore, the observed data can be obtained as the convolution between the source (J_s) and the impulse response of the earth (h_{earth}).

$$\mathbf{d}_{obs} = J_s * h_{earth} \quad (11)$$

$$J_s = IFFT(\mathbf{D}_{obs}(f) \cdot [\mathbf{D}_{mod}^{synt}(f) \cdot [J_s^{synt}(f)]^{-1}]^{-1}) \quad (12)$$

where *IFFT* is the Inverse Fourier Transform. According to Equation 12, the source can be estimated with a synthetic source with a sufficiently broad frequency bandwidth to avoid divisions by zero in the deconvolution, the modeled data, and the observed data.

The acquired raw data is shown in Figure 5A. However, to estimate the source signal, only the air-wave is needed, thus the direct arrivals are selected using an exponential time damping (Lavoué, 2014). The air-wave of the acquired data is shown in Figure 5B. The source for the GPR system is obtained using the 213 scans and it is depicted in Figure 6, which shows the source in time and the amplitude spectrum of the estimated source signal. Also, the distance from the antenna to the surface was estimated to be 0.05 m.

Data preprocessing steps

The steps used in data preprocessing include the following:

- Dewow filter: this filter selects a window and takes the mean value in the window to remove the DC components in each sample.
- Lowpass filter (LP): FWI is a local optimization technique that begins with the estimation of the low frequency components of the parameters and
- Background filter: The background filter is used to mitigate the horizontal and periodic events in the observed data, and it is called ringing noise. The ringing noise is removed using two steps, according to Khan and Al-Nuaimy (2010). The first step is to compute the eigenimages containing the highest and lowest values of the eigenvalues of the covariance matrix. The second step is to subtract the average value of the radargram. Figure 9B depicts the results when the background filter is applied to the data. The background filter is only applied in the first 500 samples where the air-wave is observed, and it avoids attenuation of some of the flat events that are of interest.
- Resampling (optional): The time step required for numerical stability is obtained using the stability condition proposed by Courant-Friedrichs-Lewy (CFL). As the spatial step is $\Delta_h=0.025$ m, we obtain that $\Delta t \leq 5.8966 \times 10^{-11}$ s. In compliance with this condition, the collected data is resampled to have a time step equal to 0.04 ns.

However, both the source and the impulse response of the earth are unknown. The impulse response of the earth can be estimated using a synthetic source and modeled data using the synthetic source (Belina et al., 2012). From the modeled and collected data, a background filter is used to select only the air wave, the details of this filter are presented in Khan and Al-Nuaimy (2010). The source is estimated from the observed data as

then the high-frequency components. Since the data is collected using a 400 MHz antenna, the radargram has been filtered using a low pass filter at 250 MHz (Figure 7). Furthermore, the source is also filtered using the same corner frequencies, which are depicted in Figure 8.

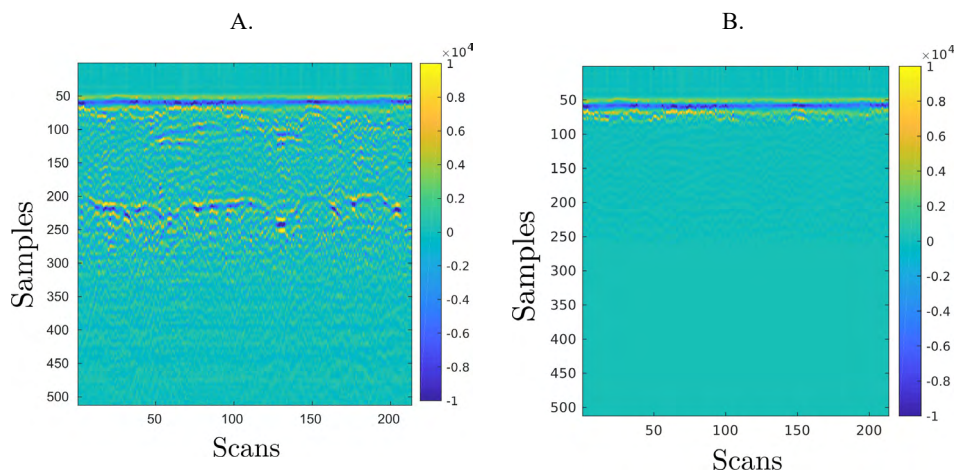


Figure 5. A. Acquired data. B. Observed data with an exponential time damping function to extract the air-wave only.

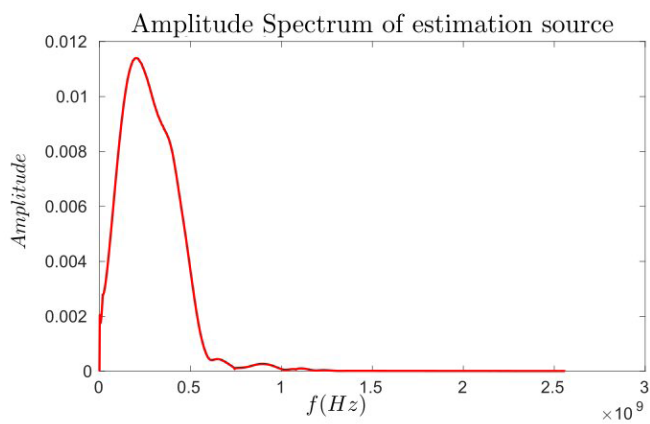
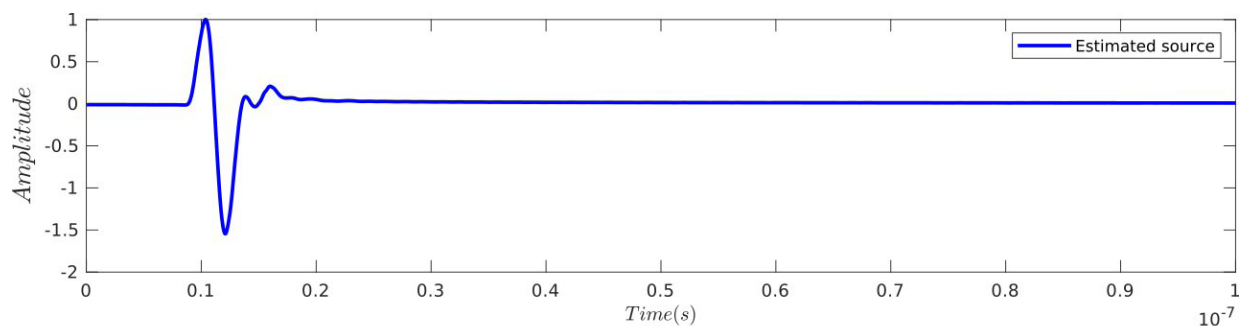


Figure 6. Estimated source and amplitude spectrum for the collected data in Mogotes.

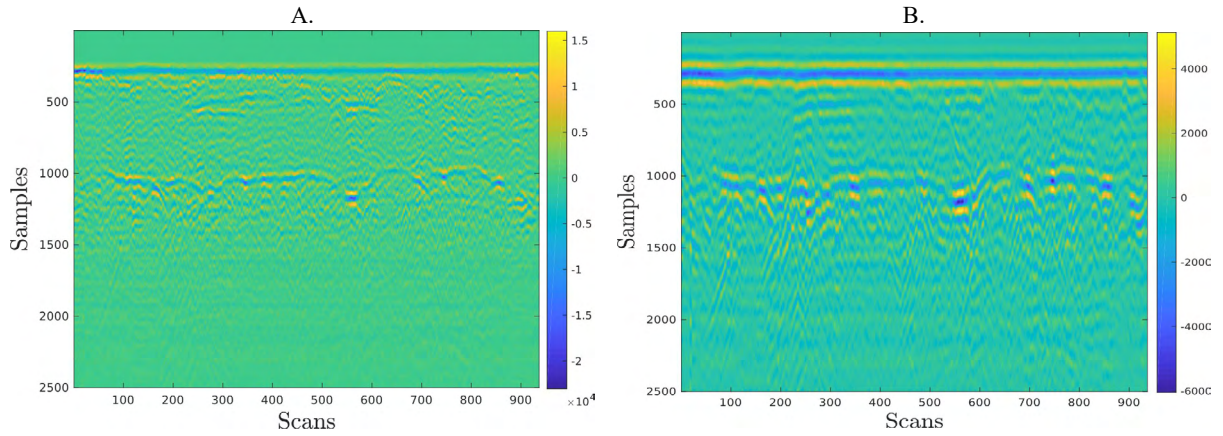


Figure 7. Collected data in the acquisition zone. **A.** Unfiltered data. **B.** Filtered data using a low pass filter between 0-250 MHz.

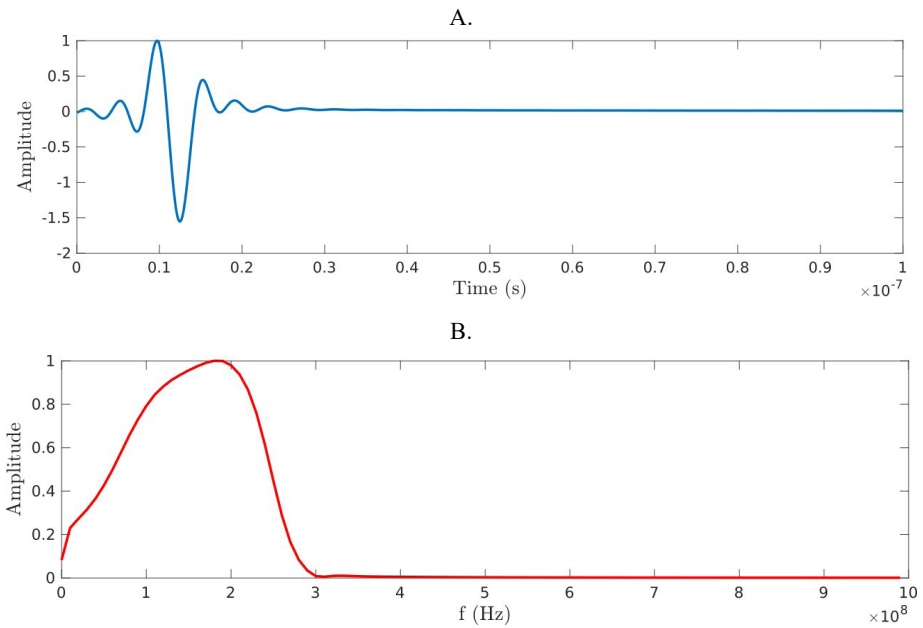


Figure 8. **A.** Filtered source in the time domain. **B.** Amplitude spectrum of the filtered source.

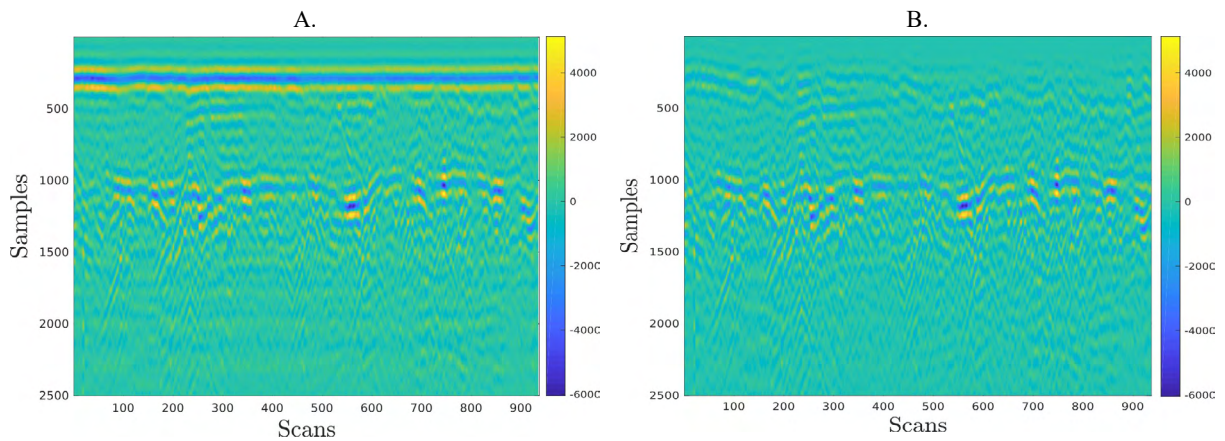


Figure 9. Background filter on the collected data. **A.** Data collected with low pass filter and without background filter. **B.** Collected data filtered with low pass filter and background filter.

FWI results using TV and MTV regularizations

TV and MTV regularizations allow for obtaining smoother solutions for the electromagnetic parameters in the inversion process. TV regularization has been included in the inversion process to analyze its behavior in the real collected data. Figure 10 shows the FWI results with TV regularization in both parameters (permittivity and conductivity). Different regularization values are tested in the experiment. Note in Figures 10B and 10G that having no regularization produces undesired values in the permittivity and conductivity parameters, which make no physical sense. In addition, to generate a smoother version of the parameters, the TV regularization does not allow extreme changes in the permittivity and conductivity values, so the inversion is more stable. Figures 10E and 10J present a very smooth solution for the conductivity parameter, so it is discarded. Similarly to TV regularization, MTV regularization is included in the inversion process. The regularization is tuned to 0.05. However, the

parameter must be tuned. Figure 11B, Figure 11C and Figure 11D, show the inversion results with MTV regularization using the values $\kappa(\sigma) = 100, 150$ and 200 , respectively. The MTV regularization converges to a less smooth model than the TV regularization. Both regularizations allow controlling the permittivity and conductivity parameters, preventing the conductivity from converging to undesired values.

FWI results with Gaussian TV and MTV regularization

TV and MTV regularization are combined in this section with the Gaussian window. The best estimation of the parameters is obtained using $q^2 = 2$ in scans-directions with a fixed window of length 66 using the FWI gradient resolution. The results of the TV regularization with a Gaussian function and the MTV with a Gaussian function are shown in Figure 12. The Gaussian window reduces the incoherent noise in the scans-direction and the solutions reach models with low-frequency information.

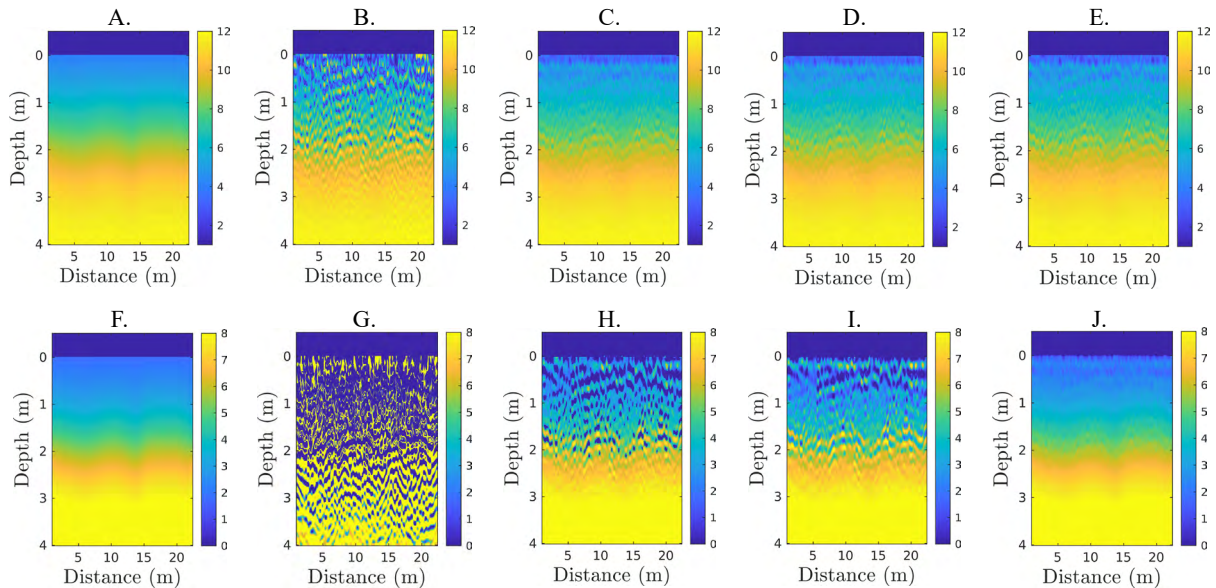


Figure 10. FWI with TV regularization, $\lambda_{TV}(\epsilon) = 5.0 \times 10^{-3}$ and $\lambda_{TV}(\sigma)$ takes values of 2.5×10^{-3} , 5.0×10^{-3} and 7.5×10^{-3} . **A.** Initial relative permittivity. **B.** Relative permittivity no regularization. **C.** Relative permittivity and TV regularization $\lambda_{TV}(\epsilon) = 5.0 \times 10^{-3}$. **D.** Relative permittivity and TV regularization $\lambda_{TV}(\epsilon) = 5.0 \times 10^{-3}$. **E.** Relative permittivity and TV regularization $\lambda_{TV}(\epsilon) = 5.0 \times 10^{-3}$. **F.** Initial relative conductivity. **G.** Relative conductivity no regularization. **H.** Relative conductivity and TV regularization $\lambda_{TV}(\sigma) = 2.5 \times 10^{-3}$. **I.** Relative conductivity and TV regularization $\lambda_{TV}(\sigma) = 5.0 \times 10^{-3}$. **J.** Relative conductivity and TV regularization $\lambda_{TV}(\sigma) = 7.5 \times 10^{-3}$.

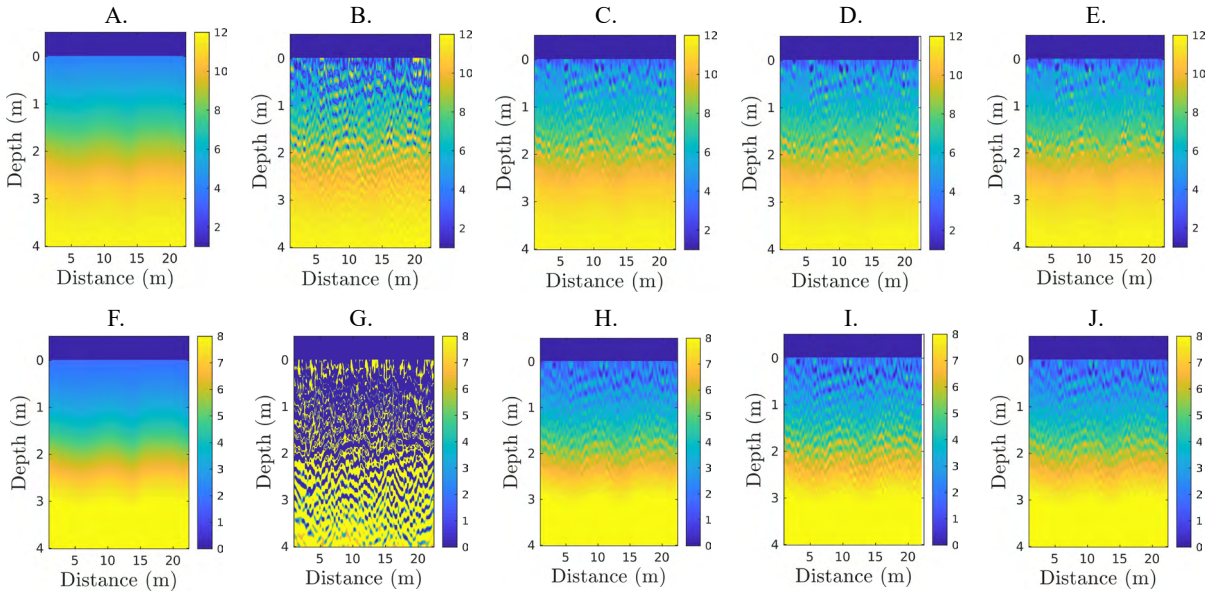


Figure 11. FWI with MTV regularization, κ takes values of 100, 150 and 200. **A.** Initial relative permittivity. **B.** Relative permittivity no regularization. **C.** Relative permittivity and MTV regularization $\kappa = 100$. **D.** Relative permittivity and MTV regularization $\kappa = 150$. **E.** Relative permittivity and MTV regularization $\kappa = 200$. **F.** Initial relative conductivity. **G.** Relative conductivity no regularization. **H.** Relative conductivity and MTV regularization $\kappa = 100$. **I.** Relative conductivity and MTV regularization $\kappa = 150$. **J.** Relative conductivity and MTV regularization $\kappa = 200$.

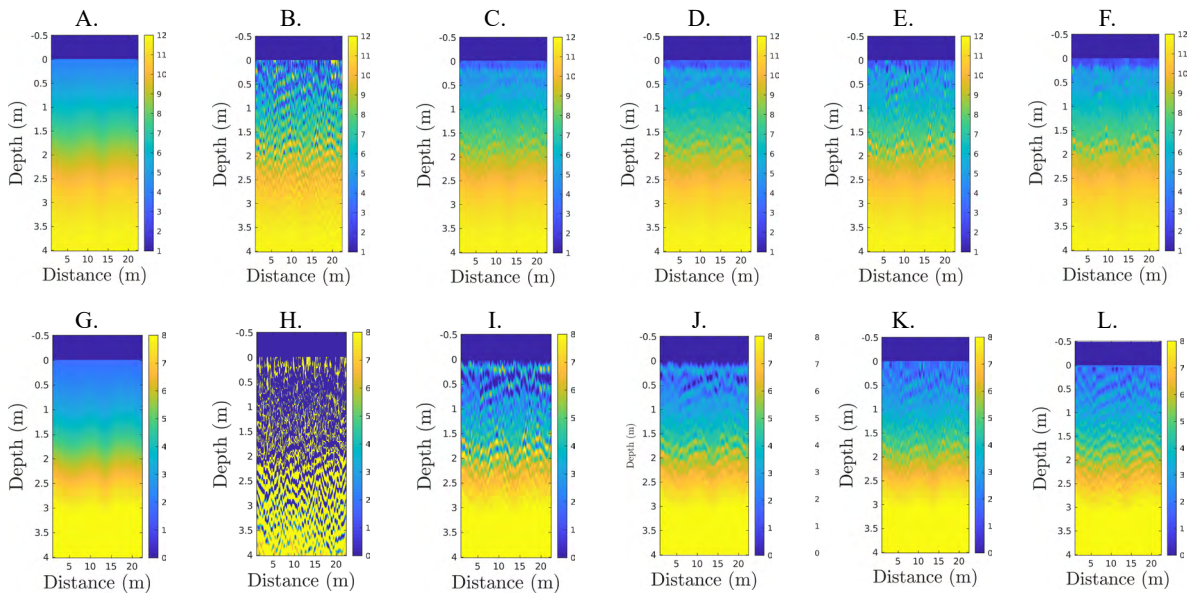


Figure 12. FWI with TV, TV+Gaussian, MTV and MTV+Gaussian. **A.** Initial relative permittivity. **B.** Relative permittivity no regularization. **C.** Relative permittivity and TV regularization. **D.** Relative permittivity and TV+Gaussian. **E.** Relative permittivity MTV regularization. **F.** Relative permittivity and MTV+Gaussian. **G.** Initial relative conductivity. **H.** Relative conductivity no regularization. **I.** Relative conductivity and TV regularization. **J.** Relative conductivity and TV+Gaussian. **K.** Relative conductivity MTV regularization. **L.** Relative conductivity and MTV+Gaussian.

Reflectivity map of the FWI results

From the reflectivity map shown in Figure 13A and Figure 13B, the coherence of the horizontal events can be observed. The reflectivity map of the underground can be obtained using Reverse Time Migration (RTM). A Laplacian filter is applied to the imaging condition to remove the low-frequency artefacts due to back-scattering in the RTM method, and a deconvolution is applied to the reflectivity map to remove the footprint of the source, such that the location of the reflector is detected. Two pairs of models of permittivity and conductivity have been used to obtain the reflectivity map: the FWI results models with the TV regularization using $\gamma_{TV}(\epsilon)=5.0\times 10^{-3}$ and $\gamma_{TV}(\sigma)=5.0\times 10^{-3}$, and the FWI results models using the MTV regularization with $\kappa_{MTV}=200$. The results of each pair of models previously described are presented in Figure 13A and Figure 13B, respectively. Figure 13 shows that the reflectivity map for the MTV model is closer to the true solution than the reflectivity map obtained with the TV model.

TV and MTV regularizations search a smooth solution that preserves the main structures of the electromagnetic

parameters. The results show that joining FWI with TV and MTV reaches a better estimation in the cost function and gives models with geological sense. The convexity in the cost function is promoted using TV and MTV regularization, it avoids being trapped in local minima with the high frequency information. However, the TV regularization is sensitive to high values in the gradient by the factor α_{TV}^2 . The results show a better estimation using MTV than TV for the conductivity values in the near-surface area, where better geologically constrained values are reached. The errors between the estimated reflectivity map and the real location of the reflectors, measured in the field, are: 1) in point A, 46 cm; 2) in point B, 14 cm and 3) in point C, 20 cm. TV and MTV regularizations, not only reduce the noise level but also preserve the primary interfaces. The experimental results show that the solution of FWI with regularization is not only smoother than traditional FWI but also the numerical result makes geological sense. Some areas of the traditional FWI solution indicate the presence of air, which is not geologically plausible.

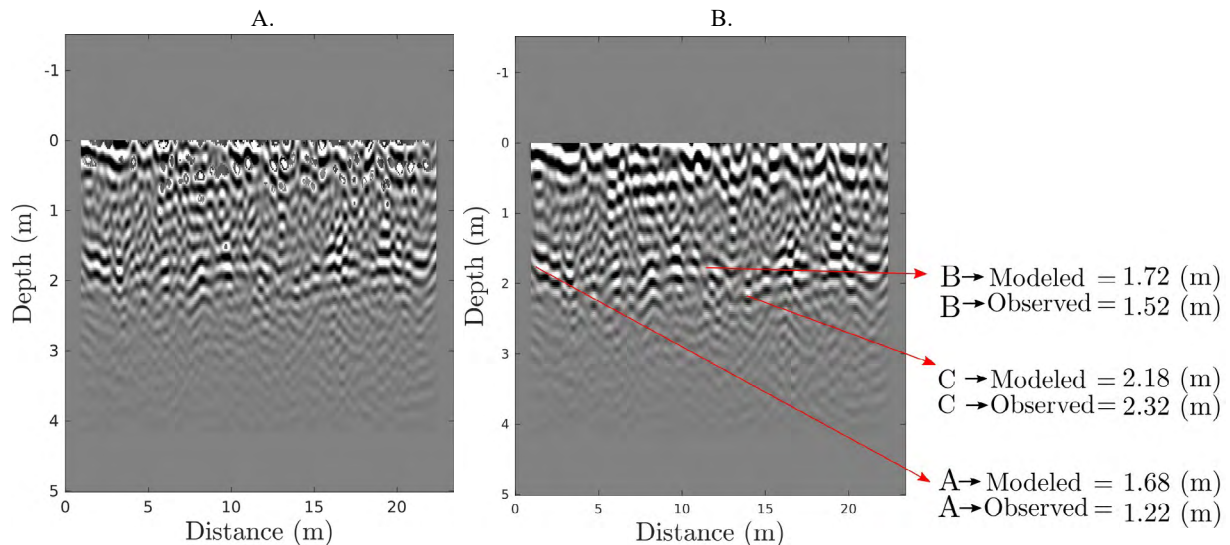


Figure 13. A. Reflectivity map for the TV models, and B. reflectivity map for the MTV models. Modeled and observed depths of points A, B and C (see Figure 2) are shown.

Summary and Conclusions

B-scan acquisitions are related to images of the subsurface that have high-frequencies. The limitation of the type of GPR system is that FWI requires an initial guess with enough low frequency information. By adding TV and MTV regularizations, the models of the electromagnetic parameters are smoother than using the typical FWI solution. Both regularizations, not only reduce the noise level but also preserve the primary interfaces.

The regularizations TV, MTV, and Gaussian window must have tuning stages of the regularization parameters such as γ_{TV} in TV, κ in MTV, or ϱ^2 at Gaussian. These parameters can be obtained experimentally using several synthetic experiments. In this work, we have also provided a set of preprocessing steps that allows preparing the data for FWI.

The experimental results show that the solution of FWI with regularization is not only smoother than traditional FWI but also the numerical result makes geological sense. Some areas of the traditional FWI solution indicate the presence of air, which is not geologically plausible. We also found that by applying the Gaussian function in the scans-direction, the incoherent noise is reduced in the data while achieving a low-wavenumber solution of the model parameters.

Acknowledgments

This research was accomplished under Grant Number W911NF-17-1-0530. The authors gratefully acknowledge the support of the CPS research group of the Industrial University of Santander, ARMY, Geophysics laboratory of the Physics School and Ecopetrol S.A.

References

- Anagaw, A.Y.; Sacchi, M.D. (2012). Edge-preserving seismic imaging using the total variation method. *Journal of Geophysics and Engineering*, 9(2), 138-146. <https://doi.org/10.1088/1742-2132/9/2/138>
- Belina, F.A.; Irving, J.; Ernst, J.R.; Holliger, K. (2012). Waveform inversion of crosshole georadar data: Influence of source wavelet variability and the suitability of a single wavelet assumption. *IEEE Transactions on Geoscience and Remote Sensing*, 50(11), 4610-4625. <https://doi.org/10.1109/TGRS.2012.2194154>
- Blom, N.; Gokhberg, A.; Fichtner, A. (2020). Seismic waveform tomography of the central and eastern Mediterranean upper mantle. *Solid Earth*, 11(2), 669-690. <https://doi.org/10.5194/se-11-669-2020>
- Bunks, C.; Saleck, F.M.; Zaleski, S.; Chavent, G. (1995). Multiscale seismic waveform inversion. *Geophysics*, 60(5), 1457-1473. <https://doi.org/10.1190/1.1443880>
- Daniels, D.J. (2004). *Ground penetrating radar*. 2nd Edition. Institution of Electrical Engineers.
- Gao, K.; Huang, L. (2019). Acoustic-and elastic-waveform inversion with total generalized p-variation regularization. *Geophysical Journal International*, 218(2), 933-957. <https://doi.org/10.1093/gji/ggz203>
- Goldstein, A. (1965). On newton's method. *Numerische Mathematik*, 7(5), 391-393. <https://doi.org/10.1007/BF01436251>
- Guasch, L.; Calderón-Agudo, O.; Tang, M.X.; Nachev, P.; Warner, M. (2020). Full-waveform inversion imaging of the human brain. *Npj Digital Medicine*, 3(1), 28. <https://doi.org/10.1038/s41746-020-0240-8>
- Jol, H.M. (2008). *Ground penetrating radar theory and applications*. Elsevier.
- Khan, U.S.; Al-Nuaimy, W. (2010). Background removal from GPR data using eigenvalues. *XIII International Conference on Ground Penetrating Radar*, Lecce, Italy. <https://doi.org/10.1109/ICGPR.2010.5550079>
- Klotzsche, A.; Van der Kruk, J.; Meles, G.A.; Doetsch, J.; Maurer, H.; Linde, N. (2010). Full-waveform inversion of cross-hole ground-penetrating radar data to characterize a gravel aquifer close to the Thur River, Switzerland. *Near Surface Geophysics*, 8(6), 635-649. <https://doi.org/10.3997/1873-0604.2010054>
- Lambot, S.; Slob, E.C.; Van den Bosch, I.; Stockbroeckx, B.; Vanclooster, M. (2004). Modeling of ground-penetrating radar for accurate characterization of subsurface electric properties. *IEEE Transactions on Geoscience and Remote Sensing*, 42(11), 2555-2568. <https://doi.org/10.1109/TGRS.2004.834800>

- Lavoué, F. (2014). 2D full waveform inversion of ground penetrating radar data: towards multiparameter imaging from surface data. PhD thesis, Université de Grenoble.
- Lin, Y.; Huang, L. (2014). Acoustic-and elastic-waveform inversion using a modified total-variation regularization scheme. *Geophysical Journal International*, 200(1), 489-502. <https://doi.org/10.1093/gji/ggu393>
- Linde, N.; Doetsch, J.A. (2010). Joint Inversion of Crosshole GPR and Seismic Traveltime Data. In: R.D. Miller, J.H. Bradford, K. Holliger (eds). *Advances in near-surface seismology and ground-penetrating radar* (pp. 1-16). SEG Library. <https://doi.org/10.1190/1.9781560802259.ch1>
- Lucka, F.; Pérez-Liva, M.; Treeby, B.E.; Cox, B.T. (2021). High resolution 3D ultrasonic breast imaging by time-domain full waveform inversion. *Inverse Problems*, 38(2), 025008. <https://doi.org/10.48550/arXiv.2102.00755>
- Mozaffari, A.; Klotzsche, A.; Warren, C.; He, G.; Giannopoulos, A.; Vereecken, H.; Van der Kruk, J. (2020). 2.5D crosshole GPR full-waveform inversion with synthetic and measured data. *Geophysics*, 85(4), H71-H82. <https://doi.org/10.1190/geo2019-0600.1>
- Persico, R. (2014). *Introduction to ground penetrating radar: inverse scattering and data processing*. John Wiley and Sons.
- Rodríguez, P. (2013). Total variation regularization algorithms for images corrupted with different noise models: a review. *Journal of Electrical and Computer Engineering*, 217021. <https://doi.org/10.1155/2013/217021>
- Rudin, L.I.; Osher, S.; Fatemi, E. (1992). Nonlinear total variation based noise removal algorithms. *Physica D: Nonlinear Phenomena*, 60(1-4), 259-268. [https://doi.org/10.1016/0167-2789\(92\)90242-F](https://doi.org/10.1016/0167-2789(92)90242-F)
- Serrano, J.O.; Ramírez, A.B.; Abreo, S.; Sadler, B.M. (2020). Alternative cost function for full waveform inversion of GPR data. *Detection and Sensing of Mines, Explosive Objects, and Obscured Targets*, 25. <https://doi.org/10.1117/12.2558605>
- Xue, Z.; Alger, N.; Fomel, S. (2016). Full-waveform inversion using smoothing kernels. *SEG Technical Program Expanded Abstracts*, Dallas, United States. <https://doi.org/10.1190/segam2016-13948739.1>

Received: 06 September 2022

Accepted: 10 May 2023
